Pergamon

PII: S0021-8502(98)00067-6

J. Aerosol Sci. Vol. 30, No. 4, pp. 439–449, 1999

Printed in Great Britain
0021-8502/99/$ – see front matter

EXPERIMENTAL AND NUMERICAL STUDIES ON THE NORMAL IMPACT OF MICROSPHERES WITH SURFACES

X. Li, P. F. Dunn* and R. M. Brach

Particle Dynamics Laboratory, Department of Aerospace and Mechanical Engineering, University of Notre Dame, Notre Dame, IN 46556, U.S.A.

(*First received* 17 *February* 1998; *and in final form* 15 *May* 1998)

Abstract—Experiments investigating the normal impact of polydisperse microspheres with surfaces have been carried out. The incident and rebound normal velocity components and particle size were measured using the phase Doppler approach. Incident normal velocities were near those required for capture by the surface. The numerical simulation approach developed by Brach and Dunn (1995, *Aerosol Sci. Technol.* **23,** 51–71), was improved and applied to analyze the polydisperse microsphere normal impact data. This improved approach was justified through comparisons with the monodisperse microsphere normal impact data of Wall *et al.* (1990, *Aerosol Sci. Technol.* **12,** 926–946) and of Dahneke (1975, *J. Colloid Interface Sci.* **51,** 58–65). © 1999 Elsevier Science Ltd. All rights reserved

1. INTRODUCTION

Microparticle impact with surfaces continues to be studied because it is involved in many important processes such as surface contamination, powder transport, coating application, etc. Although a considerable number of studies have been conducted within the last 30 years, our understanding of the deposition process is far from complete. Several models have been proposed to predict the fate of a microsphere after impact with a surface (Dahneke 1975; Wall *et al.*, 1990; Tsai *et al.*, 1991; Xu and Willeke, 1993; Andres, 1995; Brach and Dunn, 1995; etc.), yet none of them have been tested extensively by available experimental data. This is partly because most of these models require information that is not easy to quantify, such as the amount of secondary elastic deformation or the effective inertial mass of the substrate. Additional *a priori* information is required on the material properties, and, sometimes, on the surface energies. These ideally should be based on the micro-material and not on the bulk material. Unfortunately, these are not readily available.

Experimentally, Dahneke (1975) investigated the impact of monodisperse polystyrene latex microspheres with quartz targets over a rather wide range of incident normal velocities (from about 2.5 to 35 $\mathrm{m\,s^{-1}}$). At incident velocities V_{ni} below 15 $\mathrm{m\,s^{-1}}$, the coefficient of restitution, e, decreased with decreasing incident velocity, signifying the presence of adhesion effects during impact. Dahneke (1975) proposed a model to calculate the capture velocity V_{ni}^*:

$$V_{ni}^* = \left[\frac{2}{me^2}\left(E_r - e^2 E_i\right)\right]^{1/2}, \tag{1}$$

where m is the particle mass, and n the subscript denoting the normal direction. E_r and E_i are the adhesion potential energies between the particle and surface during rebound and incidence, respectively, and e is the coefficient of restitution defined by

$$e = \sqrt{\frac{\frac{1}{2}mV_{nr}^2}{\frac{1}{2}mV_{ni}^2 + E_i}}. \tag{2}$$

The requirement of knowing e and the adhesion potential energies *a priori* to determine the capture velocity prevents general application of this model. Although Dahneke (1995)

* Author to whom correspondence should be addressed.

rederived the equation for capture velocity, his new model still includes the adhesion potential energy difference and coefficient of restitution.

Wall *et al.* (1990) performed experiments to study the normal impact of four different diameters of monodisperse ammonium fluorescein microspheres (2.58, 3.42, 4.9, 6.89 μm) with four different material targets (mica, silicon, molybdenum, Tedlar). The incident velocities ranged from about 1 to 100 m s^{-1}, with adhesion effects evident below around 15 m s^{-1}. In some cases, the incident velocities were close to capture, thereby providing more confident estimates for capture velocities. By defining e as

$$e = (1 - K_l/K_i)^{1/2}, \tag{3}$$

where K_l is the kinetic energy loss during the impact and K_i is the kinetic energy for incoming particle, the capture velocity was determined from:

$$V_{ni}^{*} = (-2\Delta E/(me^2))^{1/2} \tag{4}$$

in which $\Delta E = E_r - E_i$. Dahneke (1995) pointed out that the Wall model applied to cases when $\Delta E > 0$ and his model to cases when $\Delta E < 0$.

For most practical cases, the particles deposited are not monodisperse. Dunn *et al.* (1995) reported the results of experiments on both the normal and oblique impact of polydisperse microspheres (stainless steel, silver coated glass and nickel) with planar surfaces (stainless steel, aluminium, Tedlar and copper). The normal incident velocities ranged from 2 to 25 m s^{-1}. The results were similar in behavior to the previous studies using monodisperse spheres. However, for their normal impact experiments, the incident velocities were not low enough to observe capture, as was also the case for the experiments of Wall *et al.* (1990) and Dahneke (1975).

The present study extends the work of Dunn *et al.* (1995) by investigating impact under normal incident velocities very close to capture (<2 m s^{-1}). These conditions can show more clearly the effects of adhesion and provide a better database for examining the numerical simulation method developed by Brach and Dunn (1995). Further, the improved numerical model is discussed and a systematic approach for determining the adhesion force in the model is illustrated. The numerical results of the improved model are compared with the experimental results of Wall *et al.* (1990) and of Dahneke (1975). Then, by using a polydisperse particle size distribution in the simulation, the model is applied to predict the results of polydisperse microsphere impact experiments.

2. EXPERIMENTAL APPROACH

The present experiments were conducted using the experimental system originally designed by Caylor (1993) and described by Dunn *et al.* (1995). Schematics showing the main elements of this system are given in Figs 1 and 2.

The system consisted of a vacuum test cell (maintained at 10^{-4} Torr), particle dispenser and target surface. The microspheres were dispensed by a neutral particle dispenser (NPD). Once a particle was ejected from the NPD, it was accelerated by gravity to the target surface. The vertical distance between the dispenser and the target surface varied from 0.01 to 1.0 m, providing a velocity range from 0.4 to 4.6 m s^{-1}.

A two-dimensional Phase Doppler Particle Analyzer (PDPA) was used in the 90° side-scatter mode to determine each microparticle's incident and rebound vertical velocity components and its diameter. The probe volume was positioned about 1 mm above the surface.

Type 316 stainless steel microspheres with two different size ranges were used, one from 10 to 65 μm (Duke Scientific No. 435, SST65), and another from 60 to 125 μm (Duke Scientific No. 436, SST125). A sample of the microspheres was examined using a scanning electron microscope. Their surfaces appeared "smooth" to within the resolution of the instrument. Typical size distributions of these particles, shown in Fig. 3, were measured by using the PDPA system. For all frequency and count distributions presented in this paper, the number of bins was determined according to Sturgis' rule. The target surface material

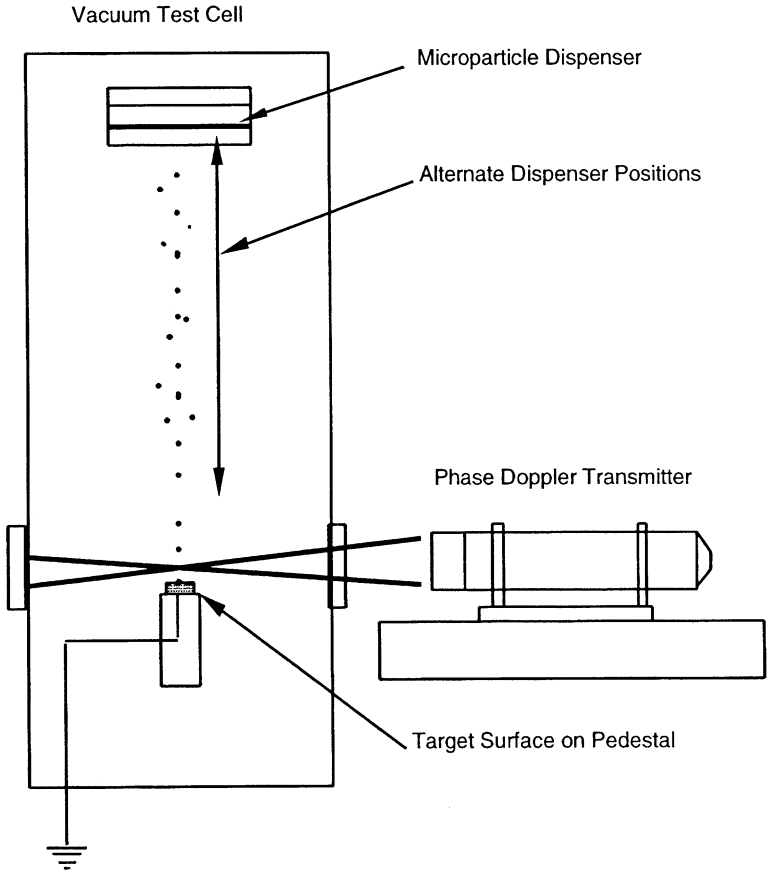

Fig. 1. Schematic of the experimental system: side view.

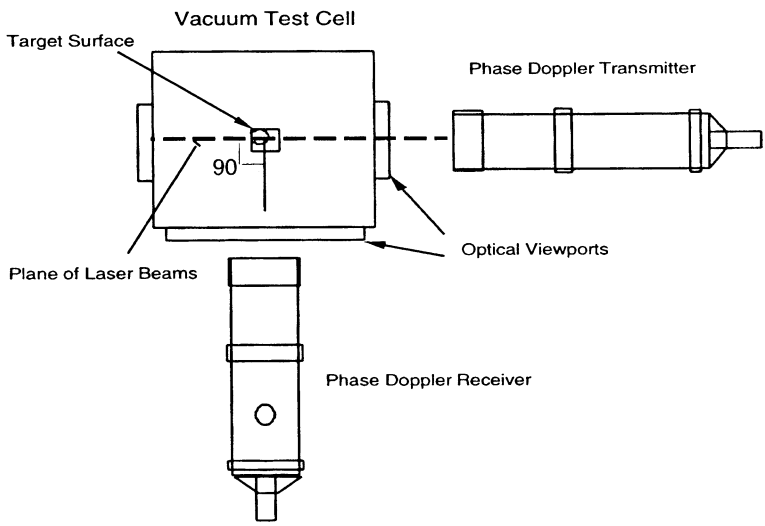

Fig. 2. Schematic of the experimental system: top view.

was an ultra-smooth (a surface asperity height standard deviation of 10 Å) $[1,0,0]$ plane silicon crystal cleaned with HF to remove the surface oxides.

During an experiment, the microsphere's vertical velocity component, diameter and time when it either entered or returned into the laser beam probe volume were recorded. After

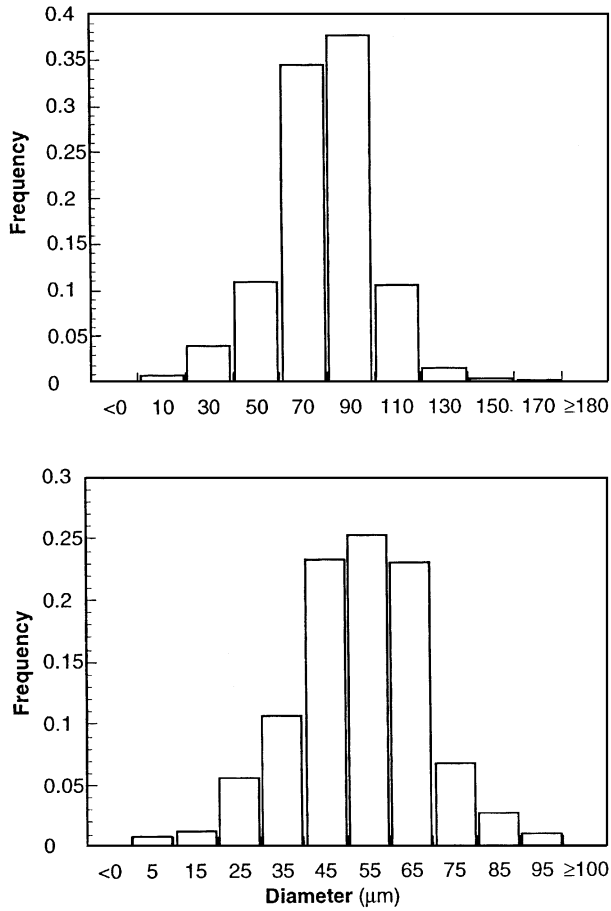

Fig. 3. Microsphere size distribution for SST125 and SST65 (note: diameter value listed under the bin is the mid-point value of the bin).

the experiment, the data was processed to identify the incident and rebound normal velocity components for the *same* microsphere. This was accomplished by using an initial estimate of the vertical distance between the laser probe volume and the target surface to initiate a pair-searching algorithm. Separate experiments were conducted to verify that the distance between the laser probe volume and the surface had no effect on pair identification. For 90° incident particles, rebound angles within $90 \pm 8^\circ$ were considered. Finally, the paired velocity data corresponding to the position of laser probe volume were corrected to give the velocity components at the surface. In this manner, the coefficient of restitution, defined as the ratio of normal rebound velocity to normal incident velocity, could be computed for each *individual* impact event and then subsequently averaged for an experiment. Usually the data from about 40 individual events were used to determine the average values.

The detail of the uncertainty analysis of PDPA measurements can be found in Caylor (1993). There is an overall uncertainty of $\pm 10\%$ for the coefficient of restitution. The uncertainties for size measurements ranged from $\pm 15\%$ for small diameters ($< 2\,\mu$m) to $\pm 1\%$ for the bigger diameters ($> 80\,\mu$m). The resulting uncertainties in the estimates of the true mean values at 95% confidence are presented in the figures by the error bars.

3. EXPERIMENTAL RESULTS

Example histograms of the normal velocity component data are presented in Fig. 4(a)–(c). The positive velocities correspond to the incoming particles; the negative ones to the rebounding ones. The data shown in Fig. 4(a) and (b) were acquired for a larger

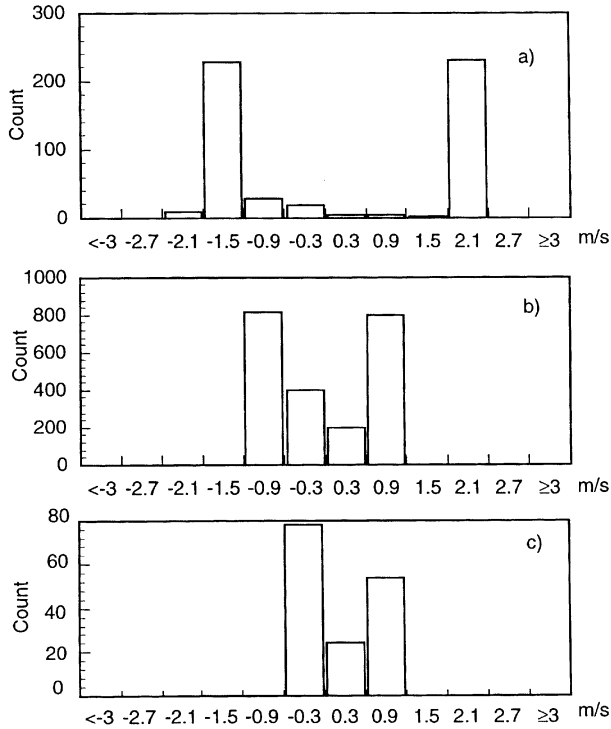

Fig. 4. Normal velocity components (a) pre-sorted data, dispenser height $h = 22$ cm, (b) pre-sorted data, $h = 4$ cm, (c) post-sorted data, $h = 4$ cm.

($h = 22$ cm) and contrasting smaller ($h = 4$ cm) particle dispenser height, respectively. The data are "raw", i.e. they have not been sorted by the pair-searching algorithm. The data displayed in Fig. 4(c) is the same as that shown in Fig. 4(b) *after* it has been sorted by the algorithm.

Figure 4(a) shows that at a larger dispenser height, the incoming velocities are centered around their free-fall velocity and that a majority of the incoming particles rebound from the surface. At a lower dispenser height, as presented in Fig. 4(b), the situation is more complicated. Some of the rebounding particles return again for a second surface impact, moving downward through the probe volume at much lower incident velocities. This tends to broaden the incident velocity spectrum. Further, some of the smaller incoming particles at these lower incident velocities are captured by the surface and prevent subsequent direct particle–surface impacts. Such ambiguities can be resolved by setting a velocity threshold in the pair-sorting algorithm. This results in an unbiased normal velocity component histogram, such as that shown in Fig. 4(c).

The two kinds of stainless steel microspheres with different size ranges yielded similar results during impact, as shown in Fig. 5. Above a certain normal incident velocity ($\sim 0.5\ \mathrm{m\,s^{-1}}$), the coefficient of restitution did not change much; below that velocity, the coefficient of restitution decreased with decreasing incident velocity. Adhesion effects were more evident for the smaller size particles (SST65) than for the larger ones (SST125). This behavior with particle size agrees with similar findings by Wall *et al.* (1990).

4. NUMERICAL SIMULATION

Brach and Dunn (1995) proposed a numerical simulation model based on Hertzian theory and a damping force model given by Hunt and Crossley (1975). They hypothesized that the adhesion force is $2\pi a f_0$, where a represents the instantaneous contact radius and f_0 the adhesion force per unit length which is assumed to be constant. This simplification of the adhesion force as a ring force follows from Johnson *et al.* (1971) (JKR theory) and

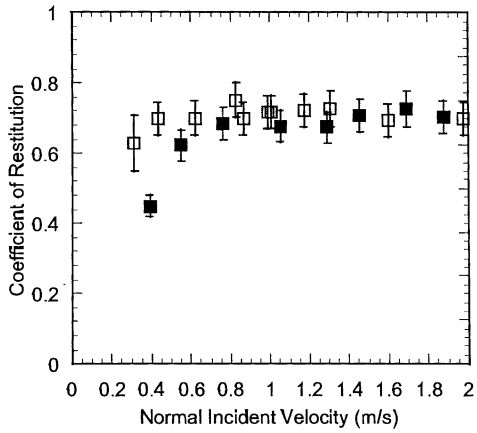

Fig. 5. Coefficient of restitution values varying with incident normal velocities [for SST125 (□) and SST65 (■)].

others. The adhesion dissipation force is strain-rate dependent, as in the Hertzian dissipation force. The governing equation of motion for the normal displacement, n, can be written as

$$m\ddot{n} = -\sqrt{r}\,Kn^{3/2}(1 + C_{\mathrm{H}}\dot{n}) + 2\pi a f_0(1 + C_{\mathrm{A}}\dot{n}), \tag{5}$$

where r is the radius and m the mass of the particle. C_{H} and C_{A} are damping factors for the Hertzian and adhesion dissipation forces, respectively. K is the appropriate Hertzian stiffness as determined by

$$K = \frac{4}{3\pi(k_1 + k_2)} \tag{6}$$

and

$$k_{\mathrm{i}} = \frac{1 - v_{\mathrm{i}}^2}{\pi E_{\mathrm{i}}} \tag{7}$$

in which v is Poisson's ratio and E is Young's modulus.

The utility of equation (5) is that it can relate f_0 directly to the static equilibrium state ($\ddot{n} = 0$ and $\dot{n} = 0$) , where

$$2\pi a_{\mathrm{eq}} f_0 = \sqrt{r}\,Kn^{3/2}. \tag{8}$$

In Hertzian theory, $a^2 = rn$, so,

$$f_0 = \frac{K}{2\pi}\frac{a_{\mathrm{eq}}^2}{r}. \tag{9}$$

Considering the adhesion deformation during contact from JKR theory (1971), the contact radius at the equilibrium state can be determined by

$$a_{\mathrm{eq}}^3 = \frac{6W_{\mathrm{A}}\pi r^2}{K}, \tag{10}$$

where W_{A} is the surface energy of adhesion, which can be approximated by $2\sqrt{\gamma_1\gamma_2}$. Here γ_1 is the free surface energy for the particle and γ_2 for the surface. Gilman (1960) presented a very simple equation for calculating the surface energy:

$$\gamma = \frac{E}{y_0}\left(\frac{a_0}{\pi}\right)^2 \tag{11}$$

in which y_0 is the equilibrium lattice constant having a value of ~2 Å, and a_0 is the elastic distance of the attractive force, having a value of ~1.3 Å. In this way, W_{A} for a given impact

system can be approximated and f_0 can be determined solely from known material properties. Equations (9)–(11) result in:

$$f_0 = (18Kr\gamma_1\gamma_2/\pi)^{1/3}. \tag{12}$$

Once f_0 is determined, only two data points are required to determine C_H and C_A using an iterative approach. One data point is chosen with a high incident normal velocity where the effects of adhesion are negligible to determine C_H. The other data point with the lowest normal incident velocity is then chosen to determine C_A. For the same materials, C_H and C_A are assumed to remain fixed. For different particle diameters, f_0 will change with radius as $f_0 \sim r^{1/3}$ according to equation (12). The application of this numerical simulation model to data obtained by Wall *et al.* (1990) and Dahneke (1975) is presented in the following.

4.1. *Numerical simulation of monodisperse microspheres*

The experimental results of Wall *et al.* (1990) from the impact of ammonium fluroscene microspheres onto silicon, molybdenum and mica surfaces can be modeled using the numerical simulation. These three experimental series were chosen because they consist of normal incident velocities over a wide range, from close to surface capture up to $\sim 100\,\mathrm{m\,s^{-1}}$. For each series, the data for a particle diameter of 4.9 μm is used to determine C_H and C_A. The parameters used in numerical simulation for $d = 4.9\,\mu$m for the three different surface materials are listed in Table 1.

All contact forces change dynamically in the simulation and are shown in Fig. 6 for the case of an incident normal velocity of $5.2\,\mathrm{m\,s^{-1}}$ for the molybdenum surface. From the simulation, it is very clear that the Hertzian dissipation force is relatively small, implying nearly perfect elastic impact, as suggested by Johnson and Pollock (1994). It is assumed that the adhesion dissipation force acts during the rebound phase. The total energy loss during the impact is mainly due to adhesion dissipation.

Table 1. Adhesion force per unit length for different impact systems

Particle material	Surface material	K (10^9 Pa)	W_A ($J\,m^{-2}$)	r (10^{-6} m)	f_0 ($N\,m^{-1}$)
Amm. fluor.	Molybdenum	1.789	0.336	2.45	8.90
Amm. fluor.	Silicon	1.776	0.216	2.45	6.60
Amm. fluor.	Mica	1.771	0.178	2.45	5.81
Polystyrene	Quartz	3.745	0.235	0.64	5.74
Stainless steel	Silicon	11.400	2.720	24.50	288.00

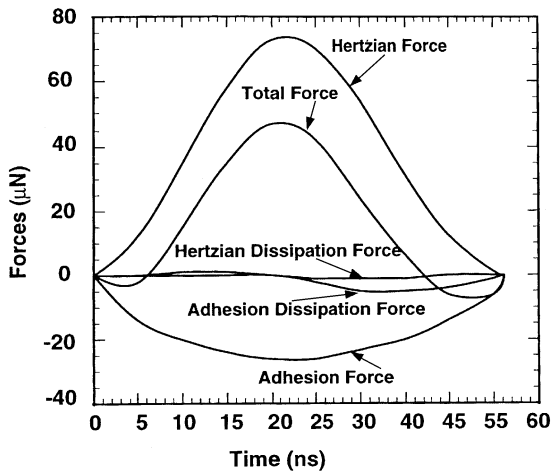

Fig. 6. Contact force variation with contact time.

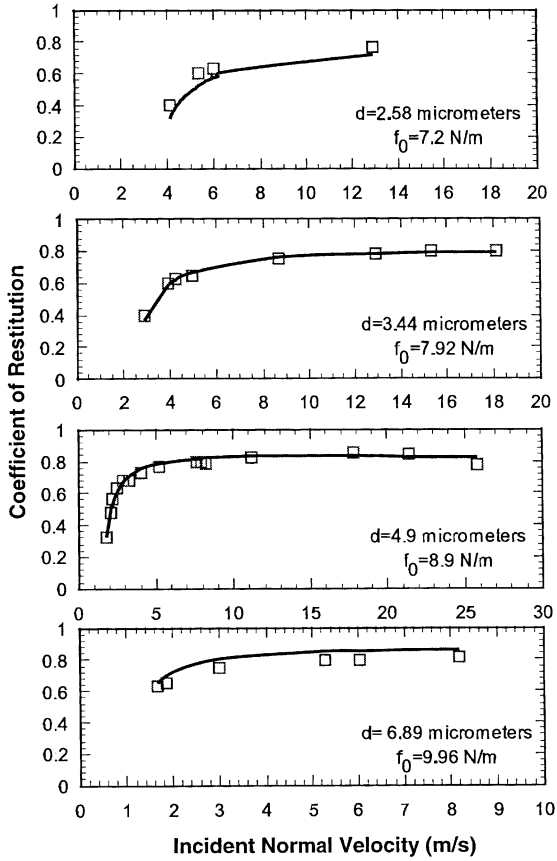

Fig. 7. Numerical simulations (——) vs experimental results (□) for molybdenum surface [data of Wall *et al.* (1990)].

After fixing C_H and C_A for each case using the values of f_0 as calculated from equation (12), the numerical simulations for the other three different sizes can be carried out. The results for the molybdenum surface case are plotted as solid lines in Fig. 7. It can be seen that for $d = 2.58\,\mu$m, the numerical predictions are slightly lower than the experimental results, but the trend of numerical results is identical to the experimental data. Similar agreement with the numerical results were obtained for the silicon and mica surface cases. The f_0's used in the numerical simulation for the different sizes of particles for the three different surface cases are shown in Fig. 8. For each curve, it can be seen that f_0 is proportional to $r^{1/3}$ exactly.

The parameter values used to simulate Dahneke's experiments are also shown in Table 1. The results are plotted in Fig. 9. The numerical simulation agrees very well with the experimental data. From these applications, it is demonstrated that this numerical simulation can be used to predict the impact of monodisperse microspheres with a surface rather well. This approach is easy to apply and only two experimental data points are needed to carry out the simulation for each material case.

4.2. *Numerical simulation of polydisperse microspheres*

Polydisperse microspheres were used for the experiments conducted in this study. For the SST65 case, the arithmetic average diameter, d_{10}, is 49 μm and the range of the distribution is from 20 to 110 μm. The parameters used for the numerical simulation for $d_{10} = 49\,\mu$m are also listed in Table 1. Using the same values of C_H and C_A for all diameters, the numerical predictions for $d = 110$ and $20\,\mu$m cases were also made. All the results are presented in Fig. 10. It is clear that the capture velocity differs significantly with particle size; the larger

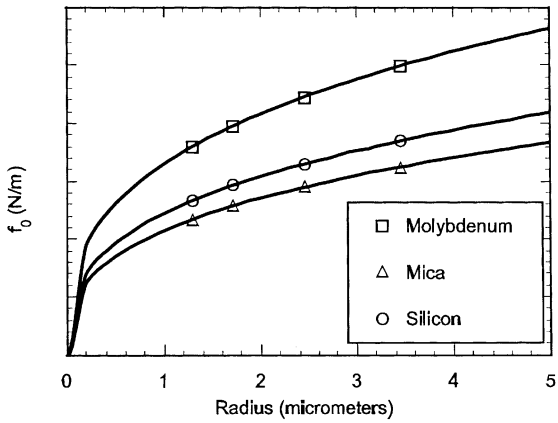

Fig. 8. Adhesion force per unit length variation with microsphere radius.

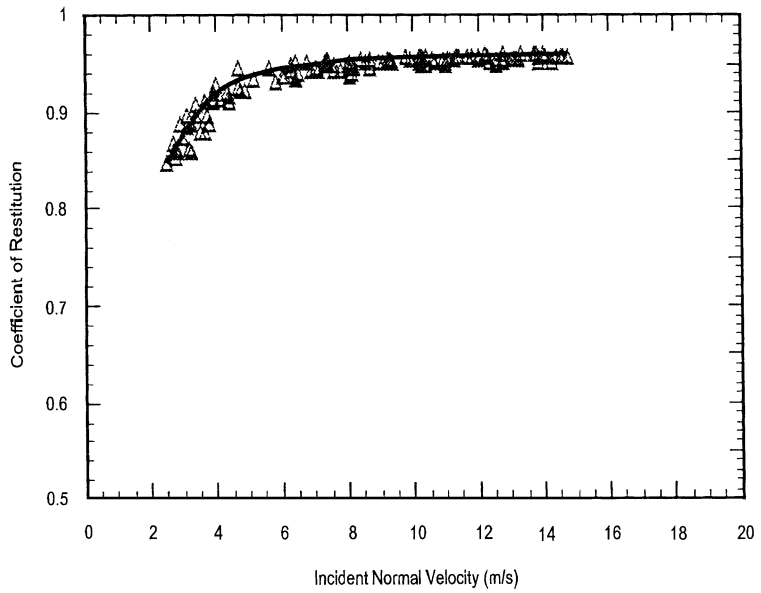

Fig. 9. Numerical simulations (——) vs experimental results (△) for quartz surface [data of Dahneke (1975)].

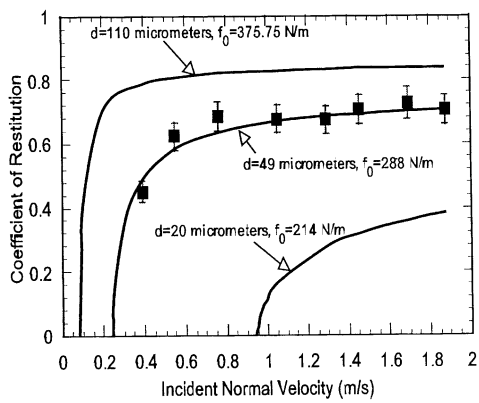

Fig. 10. Numerical simulations (——) vs experimental results for the SST65 case.

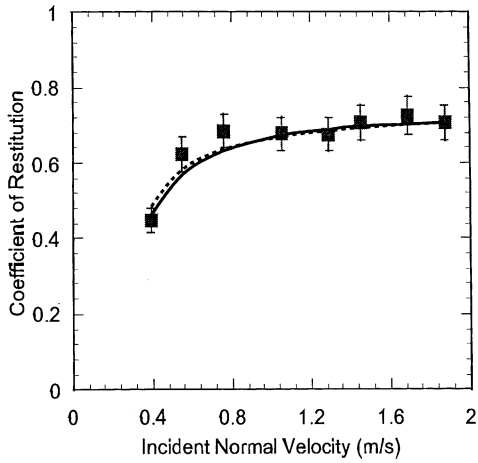

Fig. 11. Weighted average results (——) vs $d_{10} = 49\,\mu$m simulations (- - -) for the SST65 case.

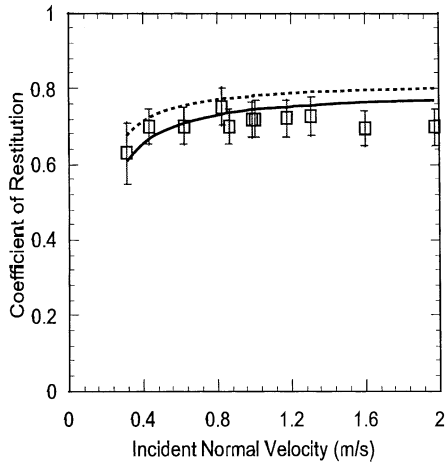

Fig. 12. Weighted average results (——) vs $d_{10} = 75\,\mu$m simulations (- - -) for the SST125 case.

the particle diameter, the smaller the capture velocity. Thus, for the SST65 polydisperse microsphere size distribution, capture occurs anywhere between ~ 0.1 and $\sim 0.9\,\mathrm{m\,s^{-1}}$. This situation can confound the results if the data is not sorted properly.

A numerical simulation based on the actual measured particle size distribution can be used to take these size effects into account. From the paired data of all of the SST65 impact experiments, a particle size distribution can be obtained. This distribution can be partitioned into 10 μm-width bins starting from 20 to 110 μm. For the median diameter of each of these bins, the numerical prediction can then be carried out by changing only f_0 according to equation (12).

Once the coefficient of restitution values are obtained from the numerical prediction for all the median diameters, an average value of the coefficient of restitution can be calculated. This average is based upon the actual number of particles in each size range, and is called the weighted average. The weighted averages are compared with the d_{10} simulation and the experimental data in Fig. 11 for the SST65 case. It can be seen that the weighted average simulation predicts the results only sightly better than the $d_{10} = 49\,\mu$m simulation at the lowest velocity because it considers particle capture. The same approach also was applied to SST125 case. These simulations and experimental data are plotted in Fig. 12, which also shows that the weighted average simulation gives better agreement with the experimental data, especially at the lower incident velocities.

5. CONCLUSIONS

The results of experiments on normal impact of polydisperse stainless steel microspheres onto a silicon surface have been reported. As observed by others, the adhesion effects at normal incident velocities close to capture were found to be more evident for smaller microspheres than for larger ones. The contribution of adhesion and its corresponding dissipation was observed to cause a noticeable decrease in the coefficient of restitution near capture. The capture velocity changed with microsphere diameter; the smaller the size, the larger the capture velocity. Due to the wide range of particle sizes used in this investigation, smaller particles captured by the surface at a higher incident velocity were shown to confound the impact results of the larger particles.

The numerical simulation approach proposed by Brach and Dunn (1995) has been improved so that the parameters in the model can be determined more systematically. This approach was verified by its successful application to the monodisperse microsphere impact results of Wall *et al.* (1990) and Dahneke (1975). Its application to polydisperse microsphere impact data also revealed that a weighted average approach can be used effectively and accurately to predict impact response.

Acknowledgements—The research described in this article was supported in part by the Center for Indoor Air Research (Contract No. 96-06) and in part by the Electric Power Research Institute (Contract No. RP 8034-03).

REFERENCES

Andres, R. P. (1995) Inelastic energy transfer in particle/surface collision. *Aerosol Sci. Technol.* **23,** 40–50.

Brach, R. M. and Dunn, P. F. (1995) Macrodynamics of microparticles. *Aerosol Sci. Technol.* **23,** 51–71.

Caylor, M. J. (1993) The impact of electrically charged microspheres with planar surfaces under vacuum conditions. Ph.D. dissertation, University of Notre Dame.

Dahneke, B. (1975) Further measurements of the bouncing of small latex spheres. *J. Colloid Interface Sci.* **51,** 58–65.

Dahneke, B. (1995) Particle Bounce or Capture–Search for an Adequate Theory: I. Conservation-of-Energy Model for a Simple Collision Process. *Aerosol Sci. Technol.* **23,** 25–39.

Dunn, P. F., Brach, R. M. and Caylor, M. J. (1995) Experiments on the low-velocity impact of microspheres with planar surface. *Aerosol Sci. Technol.* **23,** 80–95.

Gilman, J. J. (1960) Direct measurements of the surface energies of crystals. *J. Appl. Phys.* **31**(12), 2208–2218.

Hunt, K. H. and Crossley, F. R. E. (1975) Coefficient of restitution interpreted as dampling in vibroimpact. *J. Appl. Mech.* **42,** 440–445.

Johnson, K. L., Kendall, K. and Roberts, A. D. (1971) Surface energy and the contact of elastic solids. *Proc. R. Soc. London, A* **324,** 301–313.

Johnson, K. L. and Pollock, H. M. (1994) The role of adhesion in the impact of elastic spheres. *J. Adhesion Sci. Technol.* **8**(11), 1323–1332.

Tsai, C. J., Pui, D. Y. H. and Liu, B. Y. H. (1991) Elastic flattening and particle adhesion. *Aerosol Sci. Technol.* **15,** 239–255.

Wall, S., John, W., Wang, H. C. and Goren, S. L. (1990) Measurements of kinetic energy loss for particle impacting surfaces. *Aerosol Sci. Technol.* **12,** 926–946.

Xu, M. and Willeke, K. (1993) Right-angle impaction and rebound of particles. *J. Aerosol Sci.* **24,** 19–30.